

A Novel Machine Learning Algorithm for State of Health Prediction of Lithium-Ion batteries

Filippo Battaglia

*Department of Engineering,
University of Messina
Messina, Italy
fibattaglia@unime.it*

Giuseppe Campobello

*Department of Engineering,
University of Messina
Messina, Italy
gcampobello@unime.it*

Davide Aloisio

*Institute of Advanced Energy
Technologies (CNR ITAE)
Messina, Italy
aloisio@itae.cnr.it*

Salvatore Gianluca Leonardi

*Institute of Advanced Energy
Technologies (CNR ITAE)
Messina, Italy
leonardi@itae.cnr.it*

Giovanni Gugliandolo

*Department of Engineering,
University of Messina
Messina, Italy
giogugliandolo@unime.it*

Giovanni Brunaccini

*Institute of Advanced Energy
Technologies (CNR ITAE)
Messina, Italy
brunaccini@itae.cnr.it*

Francesco Sergi

*Institute of Advanced Energy
Technologies (CNR ITAE)
Messina, Italy
sergi@itae.cnr.it*

Nicola Donato

*Department of Engineering,
University of Messina
Messina, Italy
ndonato@unime.it*

Abstract—The development of Battery Management Systems (BMSs) able to determine the State of Charge (SoC) and the State of Health (SoH) of lithium-ion accumulators through a simple and cost-effective procedure is becoming of paramount importance considering their potential impact on two key enabling technologies of the 21st century, i.e., electrical mobility and energy production from renewable sources. In this paper, a novel machine-learning model, based on the Random Forest (RF) and suitable to BMS, is presented. The model is able to estimate SoC and SoH under different operating conditions by exploiting only impedance measurements derived from Electrochemical Impedance Spectroscopy (EIS). In particular, we provide an assessment of the proposed model by investigating its performance in terms of accuracy and reliability.

Index Terms—Battery Management System (BMS), Electrochemical Impedance Spectroscopy (EIS), Machine Learning, Random Forest, Battery State of Health

I. INTRODUCTION

According to the possible definitions, the State of Charge (SoC) of a battery is the ratio of the available capacity to the maximum possible charge that can be currently stored in the device. Instead, the State of Health (SoH) of a battery is the ratio of the maximum capacity that can be currently stored in the device to the maximum capacity that the device was able to store at begin of life. The development of an analytical model able to determine the State of Health (SoH) or the State of Charge (SoC) of a battery, is not a trivial task since they depend on operating conditions as well as internal chemical reactions that are quite difficult to be analyzed and modelled.

In fact, as several features of the battery, e.g., porosity and conductivity, change over time, an effective analytical model should take into account the internal structure of the battery, chemical reactions, as well as external physical parameters related to environmental and operational conditions [1]. All the parameters involved require correct definition of laws and mathematical functions of their influence on the battery behaviour as well as their possible interdependence. Therefore,

the analytical model that needs to be extracted for its description usually requires a lot of information (not always available) and deep knowledge of the system design and phenomena involved, without which the model may be very inaccurate [2]. An alternative solution to analytical models is to use data-driven approaches, currently mainstream of complex systems modelling. They don't need deep understanding of the internal mechanisms (but require large amount of data) and can provide good accuracy of the results, if well-sized [3]. Among data-driven methods, machine learning (ML) algorithms try to automatically generate models able to describe the battery behaviour, starting from training datasets. Machine learning algorithms are able to obtain black-box or grey-box models of real-world systems by exploiting dataset of previously measured input-output pairs [4]. Extensive literature is present on ML or Deep Learning (DL) techniques applied to SoC and SoH extraction [5] [6].

In this paper, with the purpose of exploring ML algorithms able to provide a good compromise between implementation complexity (directly in on-board Battery Management Systems) and accuracy, an intuitive and fast ML technique (Random Forest, RF) [7] is applied on an experimental dataset made up of impedance measures obtained using Electrochemical Impedance Spectroscopy (EIS) [8], in order to obtain SoC and SoH estimation for specific applications.

This paper is organized as follows. Sect. II describes the EIS technique. Sect. III deals with related works. Sect. IV deals with the procedure used to create the dataset that was used to train and test the proposed algorithm. Sect. V deals with the experimental results and, finally, Sect. VI deals with conclusions.

II. APPLICATION OF EIS TO LITHIUM ION BATTERIES

EIS is a characterization technique typically used to measure the impedance of an electrochemical system over a range of frequencies. The measurement method is based on the

application of a low-amplitude sinusoidal current or voltage signal of a certain amplitude and frequency, then measuring the magnitude and the shift of the voltage or current response signal, respectively [9]. In the case of lithium-ion batteries, EIS is applied for multiple purposes. For instance, it is used to study the physical and chemical processes that occur inside the cell such as charge transfer, diffusion, interfacial reactions, as well as to characterize and model the degradation phenomena of the active materials [10]. Since EIS is non-invasive analytical method, it can also provide real-time information on lithium-ion batteries as state of charge (SoC) [11], state of health (SoH) [12] and hazard conditions which can lead to thermal runaway accidents [13]. Furthermore, it can be used as a quality check tool for cell-to-cell variation due to manufacturing process [14].

Much of this information can be extrapolated by a graphical analysis of the Nyquist plot, where the imaginary part of the impedance is plotted against the real part, or from Bode plot, where magnitude and phase are plotted as a function of frequency. In fact, according to the position in the frequency range, which for lithium-ion batteries typically spans from few millihertz (mHz) to tens of kilohertz (kHz), different features and related information can be found [15].

For instance, in the upper frequency range, a typical inductive behaviour can be representative of the geometry of the cell, although artefacts from measurement must be separated. The high-frequency impedance value having phase zero, and matching with the real axis intercept in Nyquist plot, constitutes the internal resistance of the cell. This value provides information about all ohmic drops due to electrolyte, active materials, current collectors, and electrical contacts. The mid-frequency range of the impedance is representative of all electrochemical processes occurring at the electrode/electrolyte interfaces, which combine resistive and capacitive effects. This part of the impedance spectrum contains information about charge transfer kinetic at the anode and cathode, or additional layers present on the surface of the electrodes such as the solid electrolyte interphase (SEI) typically present at the anode side of the lithium-ion battery. In the Nyquist plot, these phenomena can be observed as single semicircles although often they appear as a single pseudo-semicircle due to the overlapping of the processes. Finally, the low-frequency range, which can be observed as a straight line in the Nyquist plot, is mainly representative of the lithium-ions diffusion through the electrodes and provides information on the physics of the active materials such as their porosity. Since, for a lithium-ion cell, the individual electrochemical phenomena discussed above are dependent from SoC, internal temperature, and the type of degradation undergone by the active materials due to aging, the analysis of the impedance spectrum and its evolution over time can provide information in this regard.

Although EIS is considered a powerful technique able to identify most of the electrochemical processes characterizing the lithium-ion battery behaviour, it is not frequently used for this purpose due to the complex interpretation of the data [16]. This situation is very common when the impedance data

come from an EIS measurements carried out on full lithium-ion cells, as for real-time monitoring where destructive disassembly of the cell is not practicable. In this case, the single elementary processes of both electrodes are overlapped in a single spectrum making extremely difficult its deconvolution to separate the phenomena and then extrapolate the desired information.

III. RELATED WORKS

EIS data analysis for extraction of special features describing the state of the battery can be facilitated using automated algorithms, based on equivalent circuit and physics-based model [17], mathematical approaches [18], or data-driven methods, which can extrapolate the main features and simply model the phenomena without focusing on the complex principles at the base of physical and electrochemical behaviour of the lithium-ion cells [19].

Several machine learning methods were proposed in the literature in order to obtain accurate models for Li-ion batteries, e.g., Neural Networks (NN) [20], Support Vector Machine (SVM) [21], or Fuzzy Logic [22] classifiers.

In [5] the authors presented a comparison between several ML algorithms that were used in literature to determine the SoC and SoH of a battery, such as deep learning, SVM, and convolutional neural networks (CNN). They concluded that the main drawback of deep and machine learning algorithms is the large computational burden, in particular when training is performed on a large dataset.

However, the comparison between ML algorithms presented in [5] did not consider Random Forest. As Random Forest is a ML algorithm characterized by lower computational burden than CNN and deep learning [2], it can be used advantageously for estimating SoC and SoH.

In [4] the performance of a SVM-based model was compared with the performance of two equivalent circuit models (ECMs), thus demonstrating that SVM-based algorithm achieved better accuracy than ECM models, at the cost of a higher computational cost. However, in [4] only SoC models were compared and only one kind of discharging cycle was considered. Conversely, the system proposed in this work is able to predict both SoC and SoH under different operating conditions characterized by different temperatures and different discharging cycles.

IV. EXPERIMENTAL DATASET

The experimental dataset used in this work derives from a measurement campaign carried out at the Institute of Advanced Energy Technologies (CNR ITAE) with the scope of investigating aging mechanisms in lithium-ion batteries operating under different conditions. The battery selected for this activity is a Samsung (SAMNIR) 18650-35E cylindrical cell with a high-energy density of 240 Wh/kg and a nominal capacity of 3.35 Ah. The cell consists of a Lithium-Nickel-Cobalt-Aluminium oxide (NCA) cathode and a mixed graphite/silicon anode separated by an organic liquid electrolyte. The experimental setup used for the electrical characterization, shown

TABLE I
TESTED CHARGING/DISCHARGING CYCLES

ID	Cycle	Charging	Discharging	Temperature
1	STD 0.3-1C	I=1020 mA up to 4.2 V	I=3400 mA down to 2.65 V	25°C
2	STD 0.3-1C	I=1020 mA up to 4.2 V	I=3400 mA down to 2.65 V	45°C
4	PFR	P=2.65 W, 2 min; P=5.3 W, 1 min	P=2.65 W, 2 min; P=5.3 W, 1 min	45°C
5	PFR accel	P=5.3 W, 2 min; P=10.6 W, 1 min	P=5.3 W, 2 min; P=10.6 W, 1 min	25°C
6	PFR accel	P=5.3 W, 2 min; P=10.6 W, 1 min	P=5.3 W, 2 min; P=10.6 W, 1 min	45°C
7	STD 0.6-1C	I=2040 mA up to 4.2 V	I=3400 mA down to 2.65 V	25°C
8	STD 0.6-1C	I=2040 mA up to 4.2 V	I=3400 mA down to 2.65 V	45°C
9	STD 0.6-2.5C	I=2040 mA up to 4.2 V	I=8500 mA down to 2.65 V	25°C
10	STD 0.6-2.5C	I=2040 mA up to 4.2 V	I=8500 mA down to 2.65 V	45°C
12	PFR	P=2.65 W, 2 min; P=5.3 W, 1 min	P=2.65 W, 2 min; P=5.3 W, 1 min	25°C

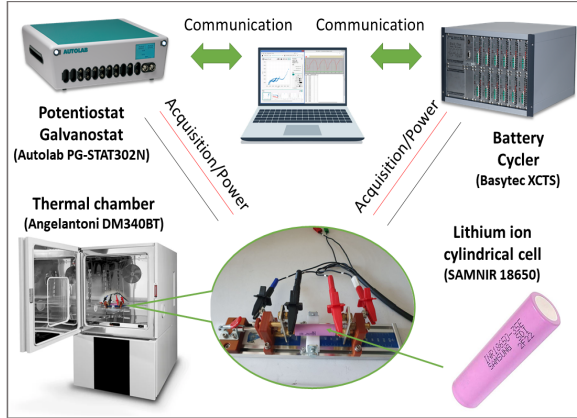


Fig. 1. Representation of battery and experimental setup.

in Fig. 1, includes a Basytec XCTS battery cycler [23] and an Autolab PGSTAT302N potentiostat [24] for the electrochemical analysis of aged cells, equipped with a multiplexer capable of managing up to 10 channels. An Angelantoni Discovery DM340BT climatic chamber was used to control the temperature during the execution of the tests, maintaining stable the required environmental conditions.

A. Ageing profiles of the cells

The measurement campaign has been carried out on 10 identical lithium-ion cells aged according to ten different operating profiles, which can be grouped in standard (STD) full charge/discharge cycles, and a power frequency regulation (PFR) endurance test as indicated by the standard IEC 61427-2 Ed.1.0 [25], reported in Fig. 2(a) and in Fig. 2(b), respectively.

The STD cycles consist of current profiles involving a constant current (CC) discharge from 100% to 0% SoC and a constant current-constant voltage (CC-CV) charge to 100% SoC, separated by 1 h rest periods. The PFR endurance test is a power profile made for large batteries, which requires that the storage system is able to provide symmetrical charging and discharging phases at constant power (CP) of 500 kW for

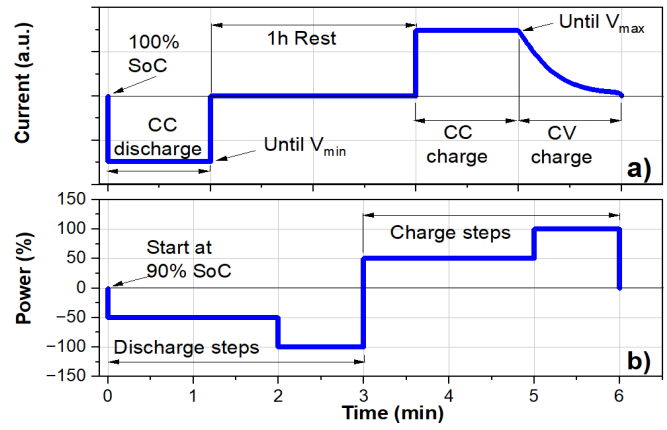


Fig. 2. (a) STD and (b) PFR aging profile

2 min and 1000 kW for 1 min, respectively. In this case, the profile was scaled down to match with maximum acceptable power for the selected lithium-ion cell. The cycle, consisting in a total duration of 6 min, was continuously repeated until the minimum voltage threshold of the cell is reached. Moreover, in order to accept the maximum power step without reaching the upper voltage threshold of the cell, the test was started at 90% SoC.

In order to evaluate the effect of two of the main stressing factors (temperature and charging rate, C-rate), both STD and PFR profiles were performed with different charge/discharge current or power (Tab. I). In particular, the test cells were subjected to three different STD cycles consisting of a manufacturer's standard cycle (0.3 C charge - 1 C discharge) and two accelerated versions at higher C-rates (0.6 C charge - 1 C discharge and 0.6 C charge - 2.5 C discharge, respectively). The other cells were subjected to two PFR profiles, one at nominal power of the cell ($P_{min}=5.3$ W, $P_{max}=10.6$ W) and the other one at a less stressful version obtained reducing by half the required power ($P_{min}=2.65$ W, $P_{max}=5.3$ W). All 5 aging cycles were carried out at 25 °C and 45 °C. In this way, a dataset with 10 classes, one for each pair of aging cycle and temperature, can be obtained.

B. Check-up tests

The SoH level of the cells was periodically monitored by dedicated parametric check-ups, performed every 25-50 cycles for STD operating profiles or approximately every 10 days for PFR endurance tests, to measure their residual capacity and internal impedance. Capacity test was performed according to the manufacturer's protocol consisting in a full charge in CC mode at 0.5 C up to 4.2 V cut-off and CV mode to 68 mA minimum current, followed by a CC discharge at 1 C up to 2.5 V cut-off voltage, both steps separated by 1 h rest at 23 °C. For a statistical analysis, the capacity test was repeated three times consecutively in order to record at least three capacity measurements for each check-up, then calculating their average value. Moreover, the capacity test was performed at 12 different aging levels and 1 time at begin of life (BoL), therefore populating the experimental dataset with 13 data points for each cell. Fig. 3 shows the evolution of

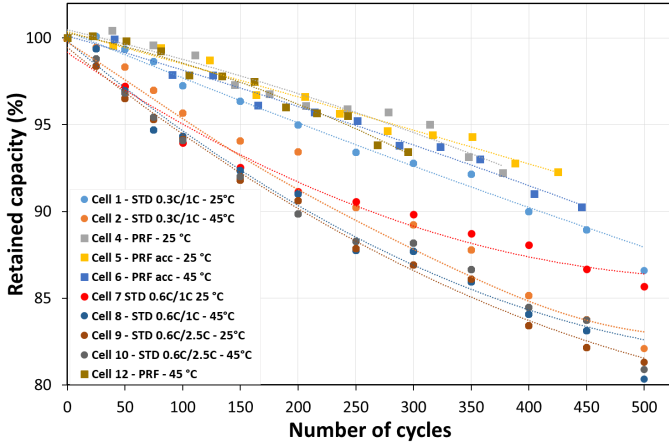


Fig. 3. Capacity loss as function of number of cycles

the capacity of the ten cells subject to the operating profiles described above as a function of the number of cycles, which matches with the actual number of cycles in the case of STD profiles. On the other hand, since the short charge/discharge steps of PRF profile do not allow the execution of full cycles, the equivalent full cycle number (N_{eq}) was used. It is defined according to Eq. 1 as the ratio between the cumulative energy supplied (E_{cd}) by the cell during the PFR test with respect to the nominal energy (E_n) of the new battery.

$$N_{eq} = \frac{E_{cd}(Wh)}{E_n(Wh)} \quad (1)$$

The cells follow a trend of capacity loss more or less marked according to the type aging profile (STD or PFR) and the related C-rate and temperature imposed. Cells 9 and 10, operating at the highest C-rate (0.6 C - 2.5 C), show greater degradation, leading to an overall capacity loss of about 17-18% after 500 full cycles. Moreover, the effect of the ambient temperature has less impact on their capacity loss. At moderate C-rate, as in the case of Cells 1 and 2 operating according to the manufacturer's profile (0.3 C - 1 C), the capacity losses at 500 full cycles are about 13% and 17%, respectively. Unlike high C-rate case, the higher operating temperature of 45 °C manifests its effects, causing a greater loss of capacity. Similar considerations can be done for Cells 7 and 8 operating at intermediate C-rate (0.6 C - 1 C), which show capacity losses at 500 full cycles of about 14% and 18%, respectively. In this case, the accelerated degradation effect induced by the higher operating temperature is still observed, although the combination of the intermediate C-rate used and the higher temperature (as for Cell 8) causes a similar loss of capacity as for Cell 10. On the other hand, Cells 4, 5, 6 and 12 aged under PRF endurance tests, show reduced capacity losses in the range 6-10%, then confirming the less degradation effect of PFR than STD cycle aging [26]. The different N_{eq} of each PFR cell in Fig. 3 is due to the different amount of energy required by each operating profile at a given test duration time.

Impedance analysis of the cells was performed by EIS technique under controlled temperature of 25 °C in potentiostatic

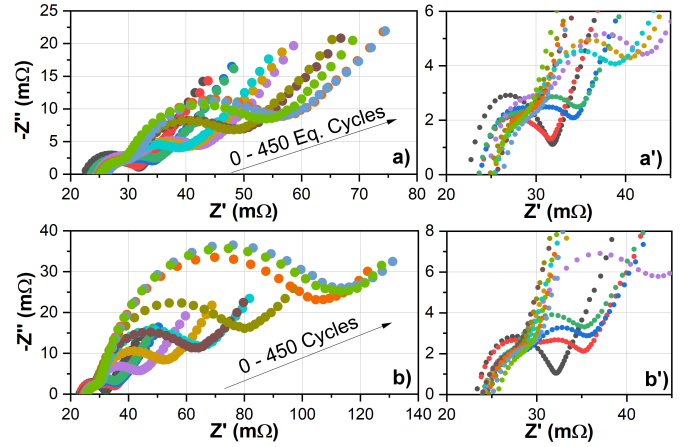


Fig. 4. Evolution of impedance with cycle aging at 100% SoC in Nyquist plots. (a) Cell 6; (b) Cell 10; (a', b') insets of high frequency regions.

mode with an amplitude signal of 10 mV. Before of each EIS measurement, the cells were allowed to reach their steady state condition (stable open circuit voltage - OCV) by waiting for at least 1 h after any external perturbation. Each cell was tested under 5 different SoC (100%, 80%, 50%, 20%, 0%) and 12 SoH levels (60 battery states in all). An EIS spectrum was recorded per each battery state (SoC; SoH), therefore the experimental dataset was populated with 60 EIS spectra per cell. OCV values recorded at the same SoC levels were also used to populate the dataset.

In a first moment, 12 cells were used, thus obtaining an experimental dataset of 720 EIS spectra in all. However, two cells were later discarded because they showed some anomalies, thus obtaining the final version of the experimental dataset made up of 600 EIS spectra related to 10 cells.

Each EIS spectrum contained the impedance measures of each cell in the frequency range 10 mHz - 10 kHz with 10 points per decade. As a result, each EIS spectrum included 60 points of impedance (real and imaginary parts) measured at 60 frequencies. Examples of EIS spectra in Nyquist plot showing the impedance evolution with PFR and STD cycle aging are reported in Fig. 4(a) for Cell 6 and in Fig. 4(b) for Cell 10, respectively. For ease of viewing, only the spectra recorded at 100% SoC and varying SoH state are shown for both cells.

The shift of the spectrum to the right is indicative of increase in the internal resistance of the cell. Furthermore, the clear separation of two semicircles in the region of medium-high frequencies, can be related with the thickening of the SEI layer and with the increase in resistance to charge transfer. The comparison between the spectra of the two cells highlights a marked difference in terms of increase of impedance with cycle aging. Similar behaviours are for all other cells of the dataset. This confirms the close correlation between cell impedance and cycle aging, which validates the EIS analysis as an optimal tool for lithium-ion cell diagnosis.

V. EXPERIMENTAL RESULTS

ML models proposed in this paper are based on Random Forest (RF) [7]. In comparison to SVM and NN, RF models require less computational power [2] and therefore are better

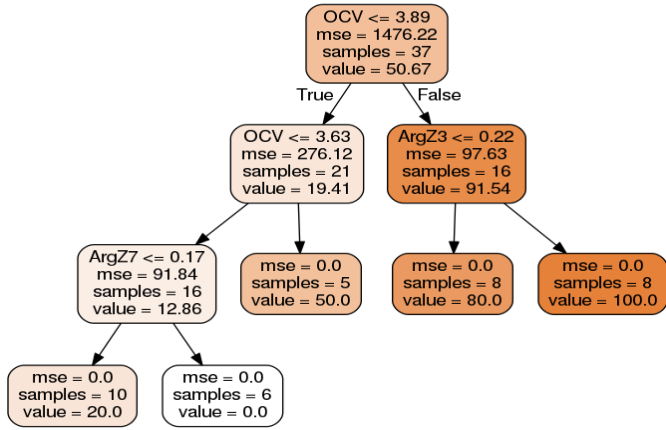


Fig. 5. The RF decision tree ($e = 5$ trees and depth $d = 4$) for SoC classification, suitable to batteries aged with the aging cycle $n_{cycle} = 1$.

TABLE II

CROSS-VALIDATION RESULTS (SOC) (RF CLASSIFIER WITH $e = 5, d = 4$)

ID	Cycle	Temperature	R2 Training	R2 Test	MAE
1	STD 0.3-1C	25°C	0.998	0.998	0.43%
2	STD 0.3-1C	45°C	0.998	0.993	0.57%
4	PFR	45°C	0.999	0.999	0.13%
5	PFR accel	25°C	0.999	0.995	0.63%
6	PFR accel	45°C	0.999	0.996	0.57%
7	STD 0.6-1C	25°C	0.997	0.992	0.80%
8	STD 0.6-1C	45°C	0.999	0.996	0.29%
9	STD 0.6-2.5C	25°C	0.999	0.998	0.33%
10	STD 0.6-2.5C	45°C	0.999	0.995	0.76%
12	PFR	25°C	0.999	0.997	0.33%
	Average		0.998	0.995	0.50%

suitable for low-cost BMSs. RF models are based on a set of decision trees optimized during the training procedure. Basically, each RF decision tree can be considered as a black box model that describes the battery behaviour under certain conditions. The final output, i.e., SoC or SoH, can be obtained by averaging the output provided by different decision trees.

The performance of RF-based models are affected by the maximum depth (d) and by the number of decision trees (e) used for the models.

Performance results reported in this section have been obtained using the dataset described in Sect. IV, considering a 80:20 cross-validation [27], i.e. by considering 5 random partitions, each made up of 80% of data used for the training set and 20% of data used for the test subset. The training subset was used to generate a set of RF models with up to $e = 5$ trees each with a maximum depth equal to $d = 4$.

The model is composed by two levels. A first level was generated in order to recognize the aging cycle (n_{cycle}) to which the cell was subjected to. The model, whose final decision tree is shown in Fig. 6, assumes as inputs the temperature and an equivalent average time T_{eq} of the battery, where T_{eq} can be calculated by dividing the overall operational time and the number of equivalent cycles N_{eq} (see eq. 1).

The second level of the model is able to predict SoC and SoH values. More precisely, ten RF models, one for each aging cycle, were generated for SoC estimation. These models exploit the open circuit voltage (OCV) and EIS features as

TABLE III
CROSS-VALIDATION RESULTS (SOH) (RF REGRESSOR WITH $e = 5, d = 4$)

ID	Cycle	Temperature	R2 Training	R2 Test	MAE
1	STD 0.3-1C	25°C	0.998	0.993	0.205%
2	STD 0.3-1C	45°C	0.996	0.990	0.332%
4	PFR	45°C	0.997	0.991	0.123%
5	PFR accel	25°C	0.997	0.991	0.158%
6	PFR accel	45°C	0.998	0.994	0.135%
7	STD 0.6-1C	25°C	0.996	0.975	0.798%
8	STD 0.6-1C	45°C	0.997	0.992	0.339%
9	STD 0.6-2.5C	25°C	0.998	0.995	0.280%
10	STD 0.6-2.5C	45°C	0.998	0.992	0.285%
12	PFR	25°C	0.999	0.996	0.095%
	Average		0.997	0.991	0.275%

input variables. As an example, in Fig. 5 the RF model used to predict SoC values for the aging cycle $n_{cycle} = 1$ is shown.

Another set of ten RF models was generated and used as SoH estimators. In this case, the number of equivalent cycles N_{eq} and EIS features have been used as input variables.

The performance of the proposed model was measured by calculating the mean absolute error (MAE) and the coefficient of determination (R2) defined respectively as follows:

$$MAE = \frac{\sum_{i=1}^n |y_i - \hat{y}_i|}{N} \quad (2)$$

$$R2 = 1 - \frac{\sum_{i=1}^n (y_i - \hat{y}_i)^2}{\sum_{i=1}^n (y_i - \bar{y})^2} \quad (3)$$

where y_i is the true value, \hat{y}_i is the value estimated by the model and $\bar{y} = \frac{1}{N} \sum_{i=1}^n y_i$.

The coefficient of determination R2 is a measure of how well a classification (regression) algorithm predicts the class (or the value) associated to a given item of the testing dataset. In general, it is bounded between 0 and 1 and greater values represent more reliable models.

Note that in Tab. II and Tab. III, R2 metric has been reported for both the training set and the test set.

The average values of MAE and R2 metrics, calculated over the 5 partitions, are shown in Tab. II and in Tab. III for SoC and SoH, respectively. As it is possible to observe, the proposed model achieves an average MAE of 0.50% and 0.275% in SoC and SoH estimation, respectively. Moreover, the coefficient of determination R2 is always higher than 0.990. This confirm the effectiveness of the proposed system.

VI. CONCLUSIONS

In this paper, we proposed a Random Forest model for estimating SoC and SoH of Li-Ion batteries. The proposed model is able to predict SoC and SoH values by exploiting values of the open circuit voltage (OCV) and a few EIS features. Experimental results show that the model is effective in determining SoC values even considering different discharging cycles. In particular, in all experiments the measured MAE was lower than 0.80% and R2 was higher than 0.992.

The system appears also to be effective in determining the SoH using as input the number of equivalent discharging cycles and EIS features. In this case, the measured MAE was

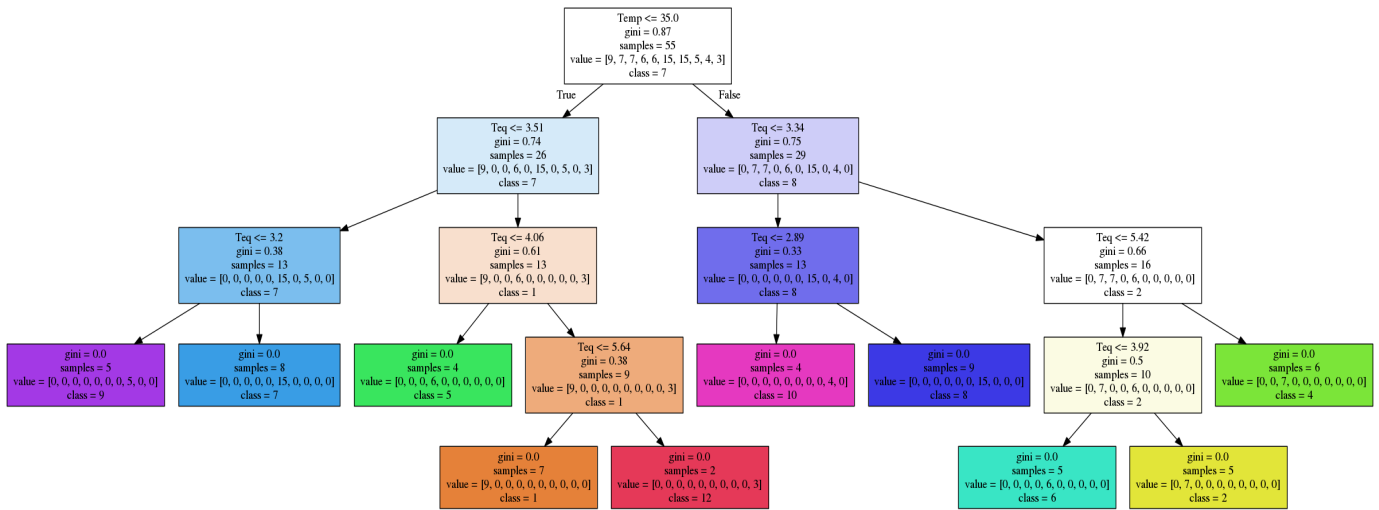


Fig. 6. The RF decision tree ($e = 5$ trees and depth $d = 4$) for aging-cycle classification.

lower than 0.798% and the achieved R2 was higher than 0.990 for all discharging cycles investigated.

As future works, the proposed model will be integrated in a BMS in order to validate its performance in a real-world and dynamic scenario.

REFERENCES

- [1] P. Carbone, A. De Angelis *et al.*, "Low-Complexity Electrochemical-Impedance Spectroscopy for Battery Monitoring," *IEEE Transactions on Instrumentation and Measurement*, vol. 72, pp. 1–9, 2023.
- [2] D. Aloisio, G. Campobello, S. Leonardi, F. Sergi, G. Brunaccini, M. Ferraro, V. Antonucci *et al.*, "Comparison of machine learning techniques for SoC and SoH evaluation from impedance data of an aged lithium ion battery," *ACTA IMEKO*, vol. 10, p. 80, 06 2021.
- [3] M. Zhang, D. Yang, J. Du, H. Sun, L. Li, L. Wang, and K. Wang, "A Review of SOH Prediction of Li-Ion Batteries Based on Data-Driven Algorithms," *Energies*, vol. 16, no. 7, p. 3167, 2023.
- [4] J. Meng, Luo *et al.*, "Overview of Lithium-Ion Battery Modeling Methods for State-of-Charge Estimation in Electrical Vehicles," *Applied Sciences*, vol. 8, p. 659, 04 2018.
- [5] Z. Ren and C. Du, "A review of machine learning state-of-charge and state-of-health estimation algorithms for lithium-ion batteries," *Energy Reports*, vol. 9, pp. 2993–3021, 2023.
- [6] M. H. Lipu, S. Ansari, M. S. Miah, S. T. Meraj, K. Hasan, A. Shihavuddin, M. Hannan, K. M. Muttaqi, and A. Hussain, "Deep learning enabled state of charge, state of health and remaining useful life estimation for smart battery management system: Methods, implementations, issues and prospects," *Journal of Energy Storage*, vol. 55, p. 105752, 2022.
- [7] M. S. Hossain Lipu, M. A. Hannan *et al.*, "Real-Time State of Charge Estimation of Lithium-Ion Batteries Using Optimized Random Forest Regression Algorithm," *IEEE Transaction on Intelligent Vehicles*, vol. 8, no. 1, pp. 639–648, 2023.
- [8] D. I. Stroe, M. Swierczynski, A. I. Stan, V. Knap *et al.*, "Diagnosis of lithium-ion batteries state-of-health based on electrochemical impedance spectroscopy technique," in *2014 IEEE Energy Conversion Congress and Exposition (ECCE)*, 2014, pp. 4576–4582.
- [9] A. Lasia, *Electrochemical impedance spectroscopy and its applications*. Springer, 2002.
- [10] P. Iurilli, C. Brivio, and V. Wood, "On the use of electrochemical impedance spectroscopy to characterize and model the aging phenomena of lithium-ion batteries: a critical review," *Journal of Power Sources*, vol. 505, p. 229860, 2021.
- [11] R. Mingant, J. Bernard, V. S. Moynot, A. Delaille, S. Mailley, J.-L. Hognon, and F. Huet, "EIS measurements for determining the SOC and SOH of Li-ion batteries," *ECS Transactions*, vol. 33, no. 39, p. 41, 2011.
- [12] X. Wang, X. Wei, Q. Chen, J. Zhu, and H. Dai, "Lithium-ion battery temperature on-line estimation based on fast impedance calculation," *Journal of Energy Storage*, vol. 26, p. 100952, 2019.
- [13] N. Lyu, Y. Jin, R. Xiong, S. Miao, and J. Gao, "Real-time overcharge warning and early thermal runaway prediction of Li-ion battery by online impedance measurement," *IEEE Transactions on Industrial Electronics*, vol. 69, no. 2, pp. 1929–1936, 2021.
- [14] K. Rumpf, M. Naumann *et al.*, "Experimental investigation of parametric cell-to-cell variation and correlation based on 1100 commercial lithium-ion cells," *Journal of Energy Storage*, vol. 14, pp. 224–243, 2017.
- [15] N. Meddings, M. Heinrich, F. Overney, J.-S. Lee, V. Ruiz, E. Napolitano, S. Seitz, G. Hinds, R. Raccichini, M. Gaberšček *et al.*, "Application of electrochemical impedance spectroscopy to commercial Li-ion cells: A review," *Journal of Power Sources*, vol. 480, p. 228742, 2020.
- [16] M. Gaberšček, "Understanding Li-based battery materials via electrochemical impedance spectroscopy," *Nature Communications*, vol. 12, no. 1, p. 6513, 2021.
- [17] N. Meddings, M. Heinrich, F. Overney, J.-S. Lee, V. Ruiz, E. Napolitano, S. Seitz, G. Hinds, R. Raccichini, M. Gaberšček *et al.*, "Application of electrochemical impedance spectroscopy to commercial Li-ion cells: A review," *Journal of Power Sources*, vol. 480, p. 228742, 2020.
- [18] B.-R. Chen, Y. R. Police, M. Li, P. R. Chinnam, T. R. Tanim, and E. J. Dufek, "A mathematical approach to survey electrochemical impedance spectroscopy for aging in lithium-ion batteries," *Frontiers in Energy Research*, vol. 11, p. 167, 2023.
- [19] M. Zhang, Y. Liu, D. Li, X. Cui, L. Wang, L. Li, and K. Wang, "Electrochemical impedance spectroscopy: A new chapter in the fast and accurate estimation of the state of health for lithium-ion batteries," *Energies*, vol. 16, no. 4, p. 1599, 2023.
- [20] P. Venugopal and V. T., "State-of-Health Estimation of Li-ion Batteries in Electric Vehicle Using IndRNN under Variable Load Condition," *Energies*, vol. 12, no. 22, 2019.
- [21] J. Meng, L. Cai, G. Luo *et al.*, "Lithium-ion battery state of health estimation with short-term current pulse test and support vector machine," *Microelectronics Reliability*, vol. 88-90, pp. 1216–1220, 2018.
- [22] P. Singh *et al.*, "Design and implementation of a fuzzy logic-based state-of-charge meter for Li-ion batteries used in portable defibrillators," *Journal of Power Sources*, vol. 162, no. 2, pp. 829–836, 2006.
- [23] BaSyTec. BaSyTec XCTS Mk II Regenerative Battery Test System. [Online]. Available: <https://www.alvatec.co.uk/energy/battery-testing/basytec/xcts-cell-test-and-formation-systems/>
- [24] Metrohm. Autolab PGSTAT302N Tech specs. [Online]. Available: https://www.metrohm.com/en_us/products/aut30/aut302n_s.html
- [25] "IEC 61427-2:2015: Secondary cells and batteries for renewable energy storage - General requirements and methods of test - Part 2: On-grid applications," Available online: <https://www.evcs.eu/en/iec-61427-2-2015>.
- [26] S. G. Leonardi, D. Aloisio, G. Brunaccini, A. Stassi, M. Ferraro *et al.*, "Investigation on the ageing mechanism for a lithium-ion cell under accelerated tests: The case of primary frequency regulation service," *Journal of Energy Storage*, vol. 41, p. 102904, 2021.
- [27] P. Refaeilzadeh, L. Tang, and H. Liu, *Cross-Validation*. Boston, MA: Springer US, 2009, pp. 532–538.